



HAL
open science

Thermo-mechanical behavior of energy diaphragm wall: Physical and numerical modelling

Shengshi Dong, Xiaozhao Li, Anh Minh A.M. Tang, Jean-Michel Pereira, van
Tri Nguyen, Ping Che, Zhiyong Xiong

► **To cite this version:**

Shengshi Dong, Xiaozhao Li, Anh Minh A.M. Tang, Jean-Michel Pereira, van Tri Nguyen, et al.. Thermo-mechanical behavior of energy diaphragm wall: Physical and numerical modelling. Applied Thermal Engineering, 2019, 146, pp.243-251. 10.1016/j.applthermaleng.2018.09.054 . hal-02877008v1

HAL Id: hal-02877008

<https://hal.science/hal-02877008v1>

Submitted on 21 Jun 2020 (v1), last revised 23 Jun 2020 (v2)

HAL is a multi-disciplinary open access archive for the deposit and dissemination of scientific research documents, whether they are published or not. The documents may come from teaching and research institutions in France or abroad, or from public or private research centers.

L'archive ouverte pluridisciplinaire **HAL**, est destinée au dépôt et à la diffusion de documents scientifiques de niveau recherche, publiés ou non, émanant des établissements d'enseignement et de recherche français ou étrangers, des laboratoires publics ou privés.

1 **Thermo-mechanical behavior of energy diaphragm wall: physical**
2 **and numerical modelling**

3 Shengshi DONG^a, Xiaozhao LI^a, Anh Minh TANG^b, Jean Michel PEREIRA^b, Van Tri

4 NGUYEN^b, Ping CHE^c, Zhiyong XIONG^a

5 *^a School of Earth Sciences and Engineering, Nanjing University, Zhugongshan Building, Xianlin*
6 *Avenue, Nanjing, Jiangsu Province 210023, PR China*

7 *^b Laboratoire Navier, UMR 8205, École des Ponts ParisTech, IFSTTAR, CNRS, UPE, France*

8 *^c East China Mineral Exploration and Development Bureau, Nanjing, Jiangsu Province 210007,*
9 *PR China*

10

11 Corresponding author:

12 Xiaozhao LI

13

14 Nanjing University

15 No.163 Xianlin Avenue, Nanjing

16 210023 Jiangsu Province

17 PR China

18 Email : lixz@nju.edu.cn

19 Phone : +86 13951604941

20 **Abstract:** The paper presents a study of the thermo-mechanical behavior of energy diaphragm
21 wall. A physical model, which consists of a small-scale concrete diaphragm wall equipped with a
22 heating exchange pipe, was used. A heating test was performed where hot water (at 50 °C) was
23 circulated through a heat exchange pipe for 75 h. The results show that the temperatures in the
24 wall and in the soil increased quickly during the first 20 h and reached stabilization at the end of
25 the experiment. Heating induced increase of axial strain in the wall and earth pressure at the
26 soil/wall interface. In addition to the experiment, a numerical model, using finite element analysis,
27 was used to predict the behavior of the wall during this experiment. The good agreement between
28 the numerical and the experimental results allows the main phenomena that took place to be
29 explained; heating induces thermal expansion of the wall that results in the modification in stress
30 in the wall and at the soil/wall interface. In addition, since the pipe was located closer to one side
31 of the wall, the thermal expansion of the wall was not homogenous, and the wall bent during
32 heating.

33 **Keywords:** Thermo-mechanical behavior; Energy diaphragm wall; Physical model; Numerical
34 simulation

35

36 **1. Introduction**

37 A thermo-active (or energy) geostructure is a new-style Ground Source Heat Pump (GHSP) system
38 that consists of conventional geostructures (*e.g.* pile foundation, tunnel lining, diaphragm wall)
39 with individual or several pipe circuits (high-density polyethylene pipes, HDPE) of primary circuit
40 embedded within to enable heat exchange with the surrounding ground [1]. In winter, heat is
41 extracted from the ground for the purpose of heating and in summer, heat is injected into the
42 ground to provide cooling. Energy geostructures are considered an interesting and promising
43 technology to tackle the increasing energy demands for heating and cooling of buildings and other
44 infrastructures, by making use of it as a local and sustainable source. However, there are still
45 concerns about the thermal exchange, between the structure and the ground, which may induce
46 variation in the stress/strain behavior of the geostructure and, as a consequence, be a threat to its
47 safety and performance. Thus, several research works have been focused on the thermo-
48 mechanical behavior of energy geostructures in order to better understand its stress/strain behavior
49 under combined thermal and mechanical loading [2-8].

50

51 However, most of the existing studies are related to the thermo-mechanical behavior of energy
52 piles. The methods used include in situ experiments [9-12], laboratory tests [13-23] and numerical
53 simulations [24-29]. It has been reported that there are significant changes in stress distribution
54 and shaft resistance due to constraints on the thermal expansion/contraction [30]. Although these
55 phenomena are not expected to lead to detrimental consequences, they should be taken into
56 consideration at the design stage.

57

58 Few studies of the thermo-mechanical performance of energy diaphragm walls have been
59 published however [31, 32]. It has been suggested that thermally-induced strains and stresses also
60 develop in energy walls [32]. However, their effects are less predictable than in energy piles
61 because of their greater complexity in terms of geometry. Sterpi *et al.* [32] performed 3D thermo-
62 mechanical Finite Element Analyses (FEA) and concluded that the thermally induced effects on
63 the structure were not negligible and could be observed partly as additional displacements, partly
64 as variations of the internal actions. Bourne-Webb *et al.* [31] also performed numerical
65 simulations and found that changes to the wall mechanical response were dominated by seasonal
66 temperature changes.

67

68 The most important function of the diaphragm wall is for ground support and seepage control. If
69 there is crack in the wall, the deformation caused by thermal expansion/contraction and lateral
70 soil pressure may aggravate the damage. Some diaphragm walls are also applied for bearing
71 purpose, as a result, the thermally-induced strains and stresses are thus important to be investigated.
72 Numerical analysis have demonstrated an increase of radial contact pressures on the soil-pile
73 interface due to temperature-induced expansion of the pile [33, 34]. For energy pile, this increase
74 of radial contact pressures could only increase the soil-pile frictional resistance. But for diaphragm
75 wall, due to the existence of excavation at one side of the wall, the pressure change may cause
76 additional deformation after Sterpi *et al.* [32]. However, the bending moment caused by heating
77 was small and overwhelmed by the effect of environmental thermal boundary conditions through

78 numerical analysis by Bourne-Webb *et al.* [31].

79

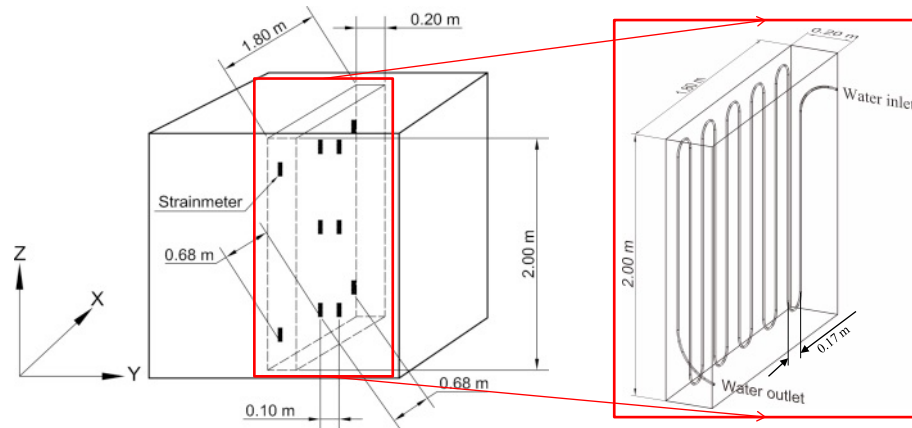
80 This paper presents a study to evaluate the thermo-mechanical response of an energy diaphragm
81 wall by using physical and numerical modeling. A small-scale energy diaphragm wall was
82 installed in dry sand. Its behavior under thermal loading was monitored using strain, stress and
83 temperature sensors embedded inside/on the wall and also in the surrounding soil. At the same
84 time, its behavior was predicted by using Finite Element Analyses (FEA). The combination of the
85 two methods allows better understanding the thermo-mechanical behavior of an energy diaphragm
86 wall when its temperature is varied.

87

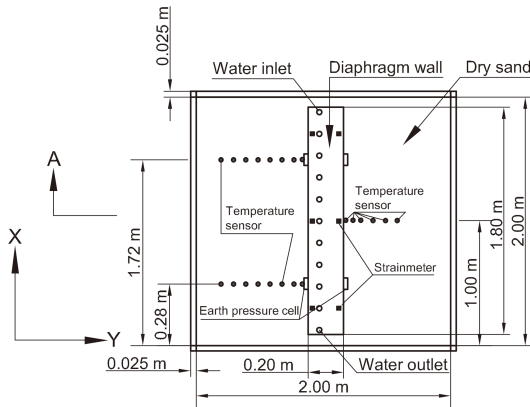
88 **2. Physical model**

89 The schematic view of the physical model is shown in Figure 1. A small-scale concrete diaphragm
90 wall (2.00 m high, 1.80 m wide, and 0.20 m thick) was installed inside a steel box and the bottom
91 of the wall was in contact with the bottom of the box. The internal height and width of the box are
92 similar to those of the wall. The thickness of the box walls and floor is 25 mm with other 30 mm
93 grillage structure outside, which is large enough to consider that the box is rigid. The box was
94 exposed to the indoor air with a controlled temperature of $10 \pm 2^\circ\text{C}$ and the heat convection
95 between the surfaces and air is natural convection. Prior to the experiment, the box was filled with
96 dry sand in layers of 0.2-m thickness which were compacted to a density of about 1.62 Mg/m^3
97 (corresponding to a relative density of 80% and void ratio of 0.63). The control of density by layer
98 ensures its uniformity throughout the test specimen. This physical model can be considered

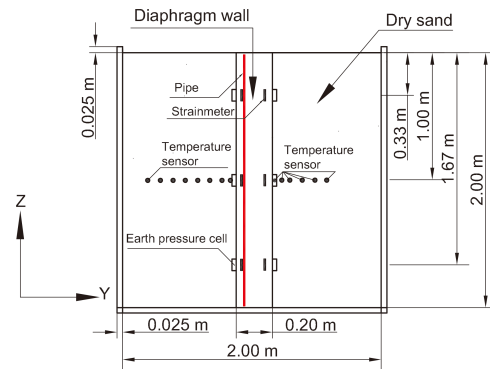
99 representative of the wall below the internal excavation level. As a result, the effect of the thermal
 100 boundary conditions on the thermo-mechanical behavior, identified in other studies [30, 31], will
 101 not be captured.



(a)



(b)



(c)

104 Fig. 1. Schematic view of the experimental setup; (a) 3D view of the physical model with the
 105 details of the pipe and strainmeters; (b) Horizontal section at $Z = 1.00$ m; (c) Section A-A, Vertical
 106 section at $X = 1.00$ m.

107

108 The soil temperature was measured at various locations located on a plane at 1-m depth (see Figure

109 1c). At this depth, the temperature sensors were distributed in three lines, two on the left-hand side
110 and one on the right-hand side (see Figure 1b). This allows the soil temperature to be measured at
111 different distances from the diaphragm wall surfaces at the same depth. The diaphragm wall was
112 equipped with high-density polyethylene pipes (10 mm in external diameter and 8 mm in internal
113 diameter) to distribute the heating fluid, and various sensors to measure earth pressure,
114 temperature and strain. The details are shown in Figures 1. The pipes were distributed on a plan
115 located at 0.05 m from the left-hand side surface of the wall and the distance between the pipes
116 was 0.17 m (see Figure 1b, c). The details of the pipe arrangement are shown in Figure 1a. To
117 measure the earth pressure at the soil/wall interface, 12 sensors were used. These sensors were
118 distributed at three depths (0.33 m, 1.00 m, and 1.67 m) (see Figure 1c). At each depth, two sensors
119 were located on each side of the wall (see Figure 1b). Several strainmeters were tied to the rebars,
120 as shown in Figure 1a, to measure the strain at various locations inside the wall. Note that the
121 strainmeters and the earth pressure transducers have integrated with thermistors to measure the
122 temperature. The characteristics of the sensors used are shown in Table 1 and the calibration and
123 correction for the temperature were done by the producers and considered in the data processing.
124 The wall was fabricated outside of the box. After 30 days of curing, it was then installed inside
125 the box and the earth pressure and soil temperature sensors were installed during the compaction
126 of dry sand to fill the box.

127

128 Table 1. Detailed information of sensors

Sensor	Market model No.	Specification	Capacity	Sensibility	Error
--------	------------------	---------------	----------	-------------	-------

Earth pressure cell	JTM-V2000	Vibrating wire	300 kPa	≤ 0.24 kPa	≤ 1 kPa
Strainmeter (embedment)	BGK-4200	Vibrating wire	3000 $\mu\epsilon$	1 $\mu\epsilon$	≤ 3 $\mu\epsilon$
Temperature sensor	Pt100	Thermal resistance	0-300 °C	$\leq 0.04\%$	0.3 °C

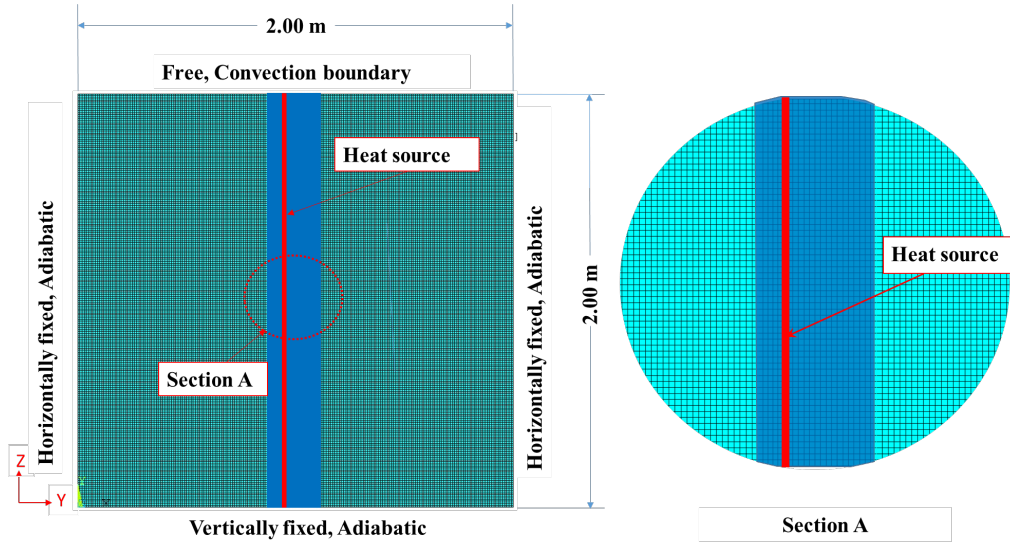
129

130 After the installation of the experiment, heating was applied to the wall by circulating water
 131 through the pipes at a temperature of 50 °C and with a flow rate of 0.03 m³/h for a period of 75 h.
 132 Beside the temperature evolution which was measured at various locations inside the wall and in
 133 the soil, earth pressures at the soil/wall interface and strains inside the wall were also recorded.

134 **3. Numerical model**

135 In order to predict the mechanical behavior of the wall during this experiment, Finite Element
 136 Analysis (FEA) (using ANSYS) was under taken. The 2D mesh, plotted in Figure 2, represents
 137 the section shown in Figure 1c. Plane strain conditions were applied corresponding to the
 138 boundary conditions of the experiment. The horizontal displacements at the left-hand side and the
 139 right-hand side were restrained. The vertical displacement at the bottom of the mesh was also
 140 restrained while the stress applied to the top of the mesh was null. The downward vertical
 141 displacement of the base of the wall was restrained but the horizontal displacement was not.
 142 According to the experimental results, the thermal boundary conditions on the left-hand side and
 143 right-hand side have only small influence on the temperature distribution. For this reason, the
 144 thermal boundary conditions on these two sides were supposed to be adiabatic. Heat flux was
 145 equally supposed to be negligible at the bottom boundary. On the top of the model, thermal

146 convection boundary was set with an air temperature of 10 °C and a convective heat transfer
 147 coefficient of 2.5 W/(m².K)([31]), as it was open to the air.



148
 149 Fig.2 Finite element mesh and boundaries conditions used for the numerical simulations.

150
 151 The governing laws used in this study are summarized as follows: (i) only conduction was
 152 considered for heat transfer; (ii) the mechanical behavior of the wall was linear elastic while that
 153 of the soil was elasto-plastic with the Drucker-Prager yield criterion; (iii) the thermo-mechanical
 154 behavior of the wall and soil was linear elastic. The material parameters used for the simulation
 155 are shown in the Table 2. Among the parameters, the density, thermal conductivity and specific
 156 heat of cement mortar and sand used in the FEA were measured by specialized equipment and
 157 also calibrated by one dimensional finite difference method with MATLAB. The Young's
 158 modulus and Poisson's ratio of cement mortar were measured by elastic modulus test machine.
 159 Other parameters of cement mortar and sand were taken from the literatures ([35-37]). It should

160 be stated that the coefficient of linear expansion was chosen at $0.6 \times 10^{-5} \text{ } ^\circ\text{C}^{-1}$ from literature [35],
 161 which gives a typical linear thermal expansion coefficient for dense quartzose sands from 0.6×10^{-5}
 162 $^\circ\text{C}^{-1}$ to $2.0 \times 10^{-5} \text{ } ^\circ\text{C}^{-1}$. The lowest value was chosen to examine the effects of soil thermal
 163 expansion on the thermal-mechanical behavior of the wall. For the friction angle, there are
 164 literatures which give $30\text{-}36^\circ$ from loose sand to dense sand [36, 38], we chose 30° as it's density
 165 may not easy to compacted to the design stage of the lower depth. According to literature review
 166 [36], the dilation angle of dense sand and loose sand are from $0\text{-}12^\circ$ and $0\text{-}10^\circ$, respectively. It
 167 was chosen at 4° as an intermediate value in the present study.

168

169 Table 2. Materials parameters used for simulation

Parameter	Cement mortar	Dry sand
Thermal conductivity (W/(m.K))	1.20	0.32
Density (Mg/m ³)	1.55	1.62
Specific heat (J/(kg.K))	736	700
Young's modulus (MPa)	12,000	50
Poisson's ratio (-)	0.20	0.23
Coefficient of linear expansion ($\mu\epsilon/^\circ\text{C}$)	10	6
Cohesion (kPa)	—	0.1
Friction angle ($^\circ$)	—	30
Dilation angle ($^\circ$)	—	4

170

171 In order to simulate the heating phase performed in the experiment, the temperature of the pipes
172 (the vertical line located inside the wall, see Figure 2) was imposed. The initial temperature of
173 the whole system was first fixed at 10 °C (following the experimental observation). To start the
174 heating phase, the temperature of the pipe was increased from 10 °C to 48.5 °C following
175 function (1):

$$176 \quad T = \frac{2.07 \bullet t + 1.1615}{0.0414 \bullet t + 0.12323} \quad (1)$$

177 where t is elapsed time and T is temperature. This choice allows fitting the experimental data of
178 the temperature measured by the sensor that is closest to the pipes (0.03 m from the pipe axis, on
179 the left-hand side).

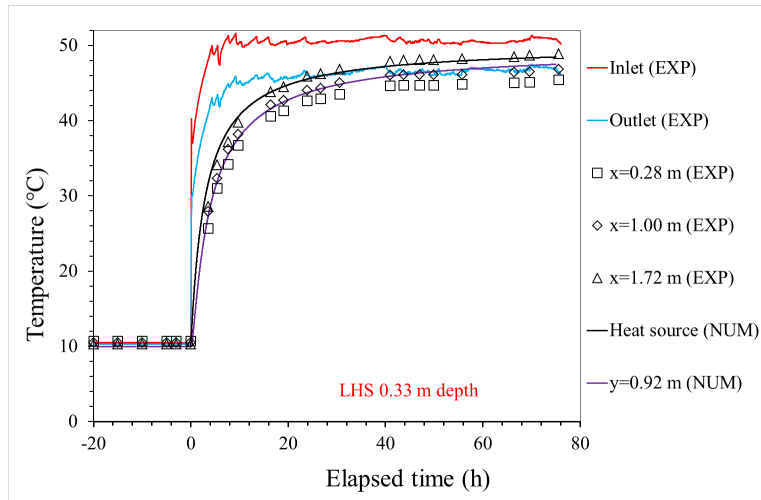
180 **4. Result**

181 In this section, the results obtained from physical test and numerical analysis are compared in the
182 same figures.

183 Figure 3 shows the temperature measured within the wall on the left-hand side in the plane of the
184 wall panel at three different depths (0.33 m, 1.00 m and 1.67 m) and on the right-hand side at mid-
185 plane ($x = 1.00$ m Fig.1) versus elapsed time (the origin corresponds to the start of the heating
186 phase). The symbols represent the experimental data (EXP) and the continuous lines represent the
187 numerical results (NUM). Note that in the experiments, more than one sensor exists for one
188 distance (see Figure 1b). As an example, at $y=0.92$ m on the left-hand side (Figure 3) within the
189 wall, there are three sensors on each depth (0.33 m and 1.67 m). The results obtained by these
190 three sensors (showing an increase of temperature from 10 °C to 45 °C) have a difference of about

191 3-4 °C at the end of the heating phase. This difference can be explained by the gradual cooling of
192 the fluid while circulating into the pipe which represents an ordinary characteristic condition of
193 energy diaphragm wall.

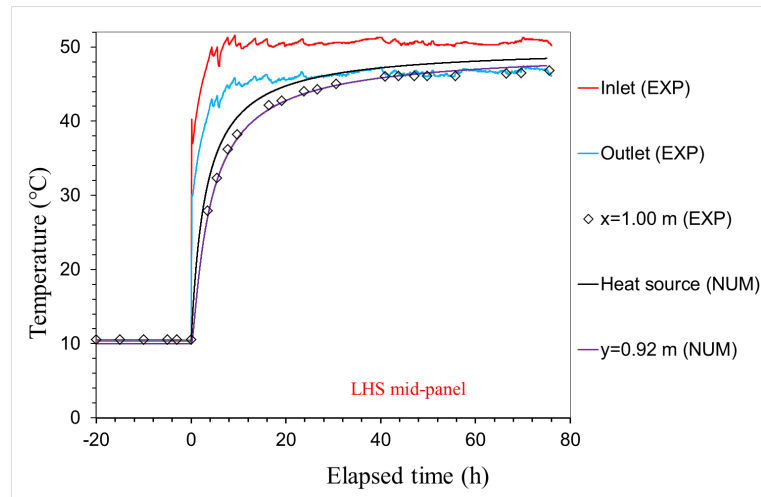
194



195

196

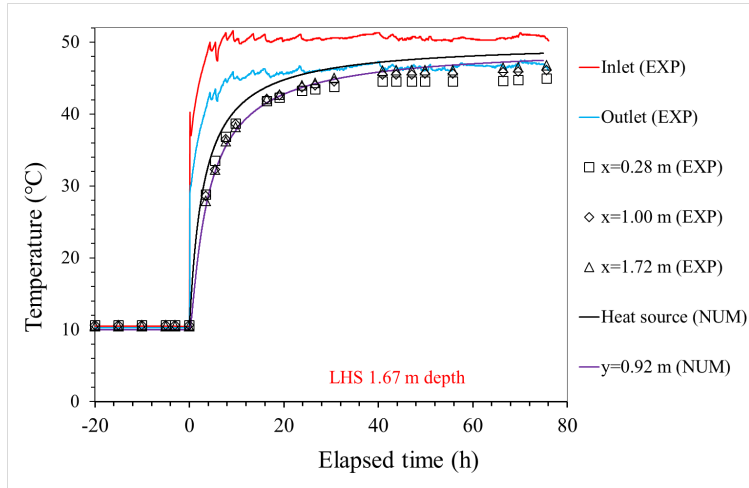
(a)



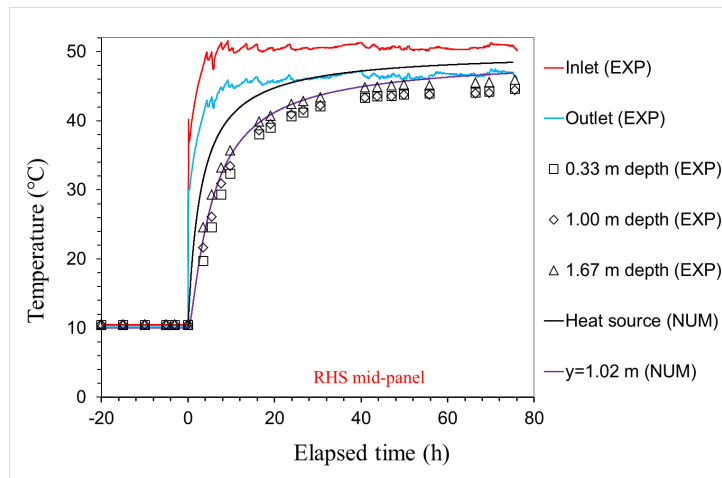
197

198

(b)



(c)



(d)

199
200

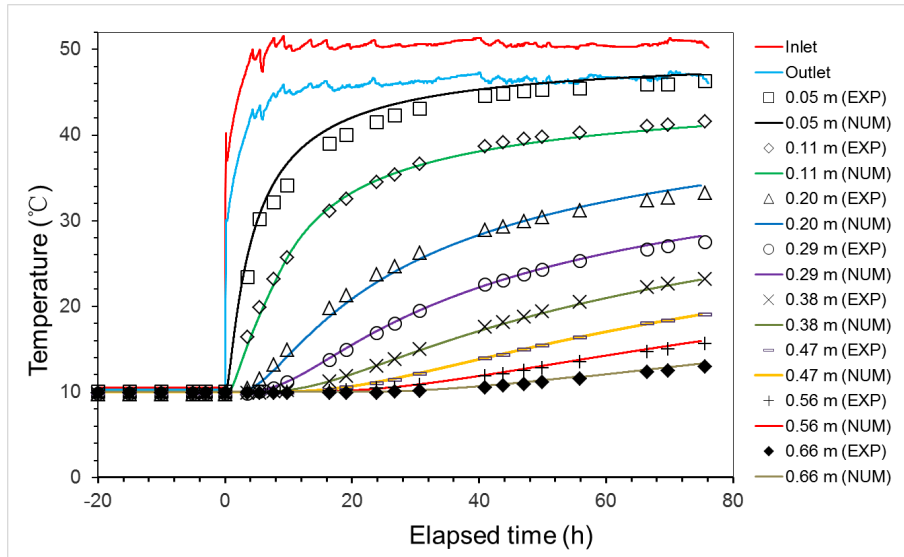
201
202

203 Fig.3. Temperature versus elapsed time within the wall on the left-hand side along the x
204 coordinate at depth of (a) 0.33 m and (b) 1.00 m and (c) 1.67 m and on the right-hand side at
205 $x=1.00$ m for various depths (d)

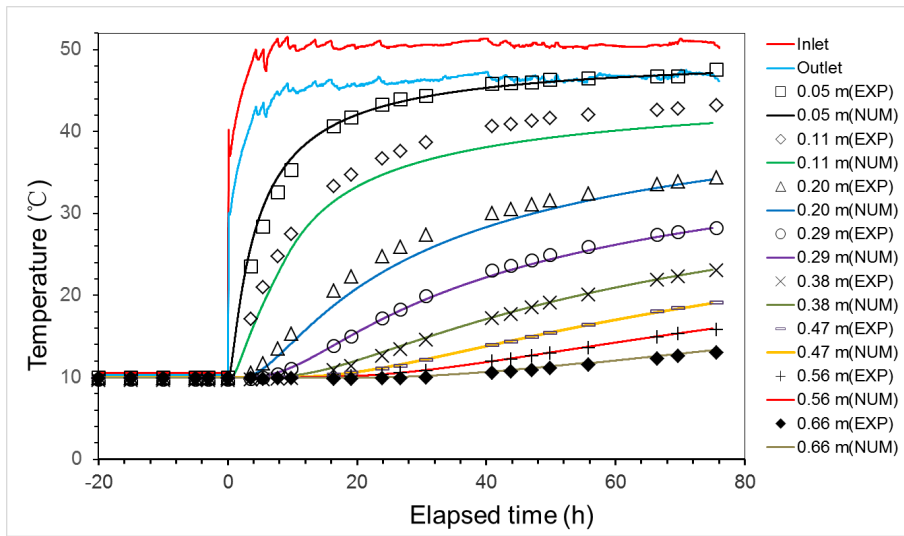
206

207 Figure 4 shows the temperature for each single line of sensors embedded in the sand. The
208 agreement between the experimental data and the numerical results confirms that the numerical
209 2D finite element model is suitable to predict the heat transfer in sand in this experiment.

210



(a)



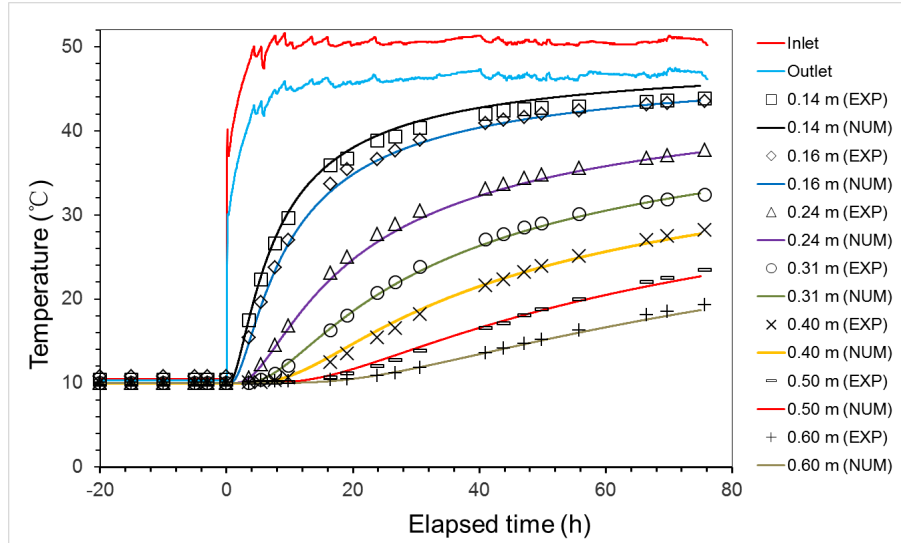
(b)

211

212

213

214



(c)

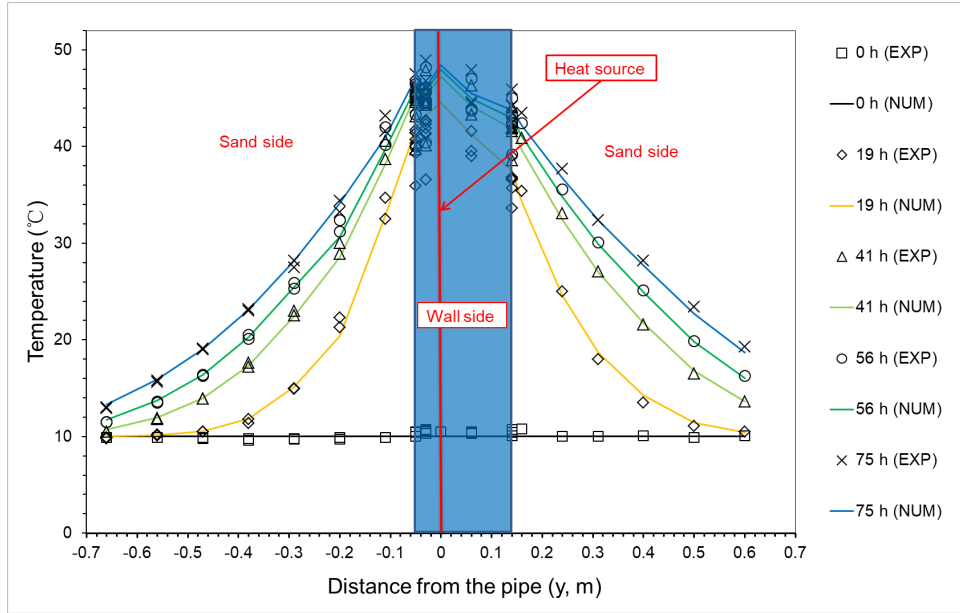
215

216

217 Fig.4. Temperature versus elapsed time in the sand mass at various distances from the pipes
 218 axis: (a) on the left-hand side at $x = 0.44$ m; (b) on the left hand side at $x = 1.56$ m; (c) and on
 219 the right-hand side at $x = 1.00$ m.

220

221 Figure 5 shows the temperature profile measured at various moments. It can be seen that at a given
 222 time, the temperature at a location closer to the pipe is higher. This plot allows two zones to be
 223 distinguished: inside the wall, the temperature gradient is smaller than in the soil. That can be
 224 explained by the thermal conductivities of these materials and the boundary conditions: the wall,
 225 made of cement, is more conductive than the sand and therefore, the temperature gradient is then
 226 smaller.



227

228 Fig.5 Temperature versus distance from the pipe at various elapsed times in the middle of the
 229 panel ($z=1.00$ m)

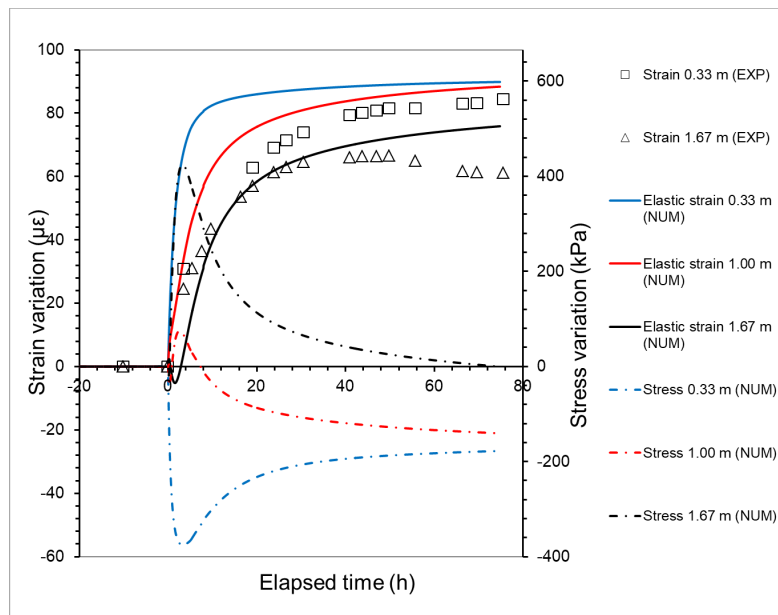
230

231 The numerical results shown in Figures 3, 4 and 5 are in good agreement with the experimental
 232 results. That confirms, in this experiment, heat transfer is mainly governed by heat conduction (as
 233 considered in the numerical simulation). This agreement confirms also that the thermal boundary
 234 conditions used in the simulation are acceptable. In addition, as a 2D mesh was used in the
 235 simulation, the numerical results should be compared with the mean values obtained in the
 236 experiments with various sensors located at the same distance. The non-uniform of the
 237 temperature distribution along the X direction (observed from the experiments) can be ignored in
 238 the numerical model.

239

240 Figure 6 shows the vertical strain (Z direction, see Figure 1a) measured at various x coordinates
 241 by the strainmeters. Note that all the strainmeters on the left-hand side (Figure 6a, 6b and 6c) are
 242 located 0.03 m from the pipe. The results show similar trends for all sensors; a rapid increase of
 243 strain during the first 20 h (corresponding to the increase of fluid temperature during the
 244 experiment) followed by a more stable phase. The final strain is in the range of 50-70 $\mu\epsilon$ (except
 245 one sensor at 0.33-m depth). The three sensors located at 0.33-m depth show larger strain variation
 246 than those at 1.67-m depth; there is only one sensor located at 1.00-m depth. On the right-hand
 247 side (Figure 6d), only one sensor was used for each depth. Note that these sensors are located 0.06
 248 m to the right-hand side of the pipes. The results obtained by these sensors are quite similar
 249 showing a quick increase during the first 20 h and stabilization at 55 - 65 $\mu\epsilon$. These discrepancies
 250 in strains can be directly linked to the heterogeneity of temperature distribution of the wall shown
 251 in Figure 6.

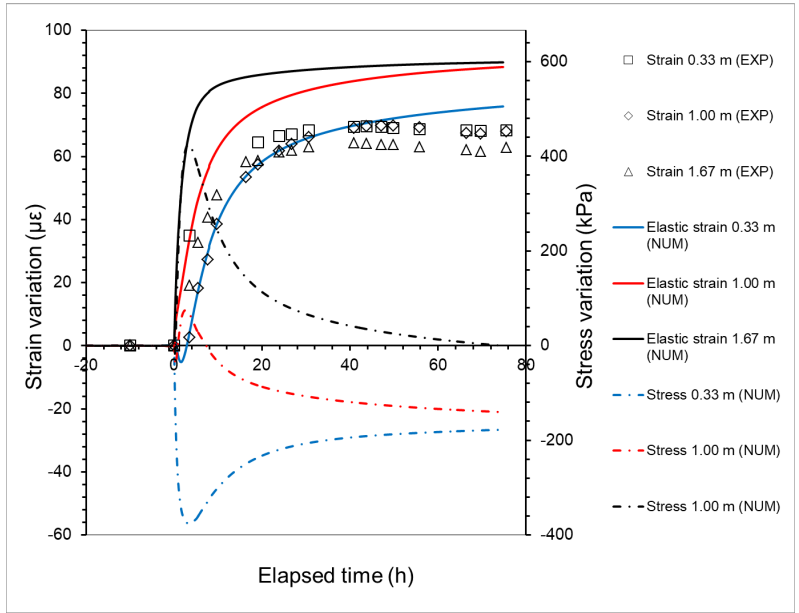
252



253

254

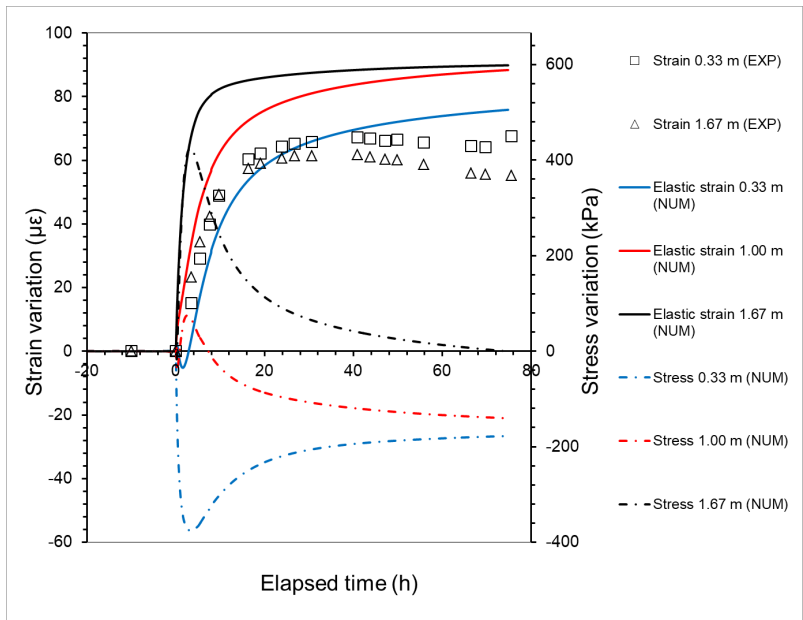
(a)



255

256

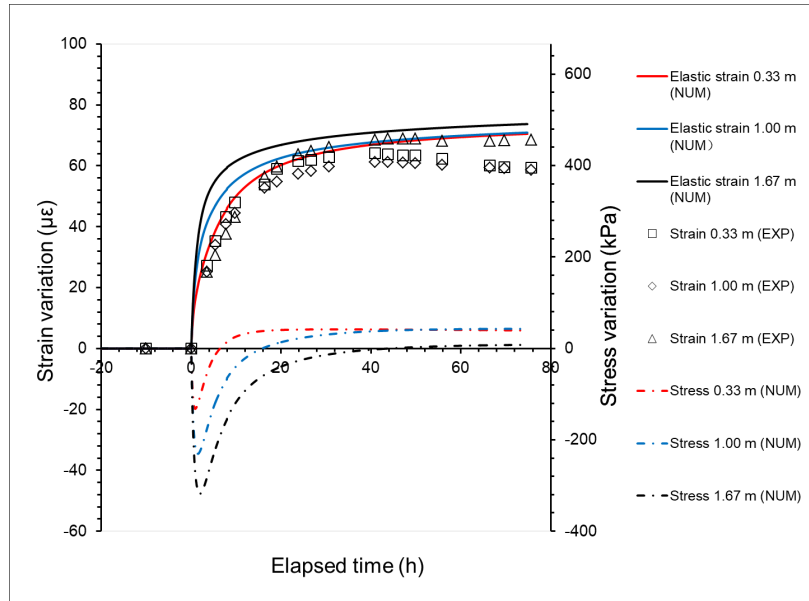
(b)



257

258

(c)



(d)

259

260

261 Fig.6. Vertical strain and stress versus elapsed time on the left-hand side at (a) $x=0.28$ m ; (b) x
 262 = 1.00 m ; (c) $x=1.72$ m ; (d) and on the right hand at $x=1.00$ m.

263

264

265 The vertical strains predicted by the numerical analysis are also shown in the Figure 6 (positive
 266 strain corresponds to expansion). On the left-hand side, the numerical analysis show that heating
 267 induced a quick expansion at 0.33-m depth followed by stabilization at $80 \mu\epsilon$. This result is similar
 268 to that obtained by the experiment. However, for the other depth (1.67 m), the numerical analysis
 269 shows a contraction during the first hours. This contraction was then followed by expansion and
 270 the final values are also similar to the experimental ones. The trend of the vertical strains on the
 271 right-hand side shows a good agreement between the numerical and the experimental results.

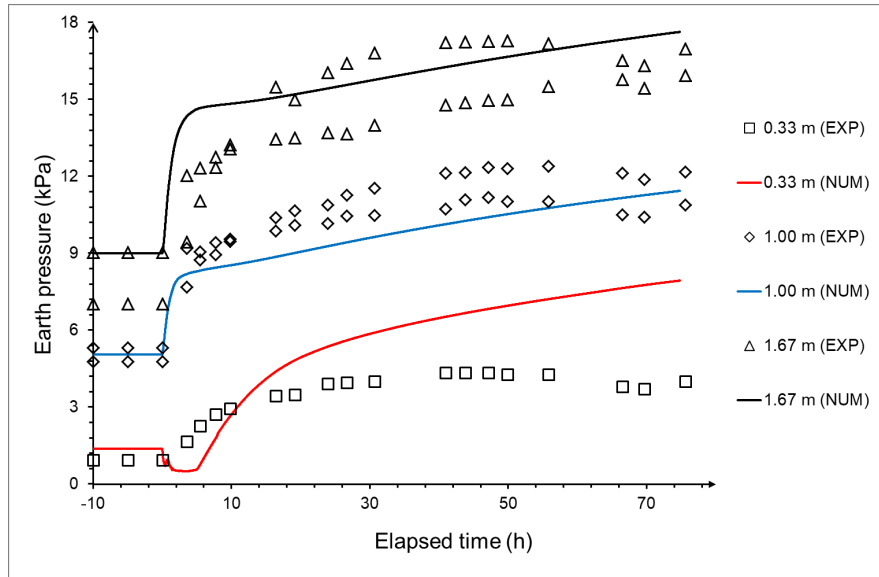
272

273 The following mechanisms can be mentioned to explain these results (see also the vertical stress
274 variation plotted in the Figure 6). The high value of vertical stress is related to the temperature
275 gradient in the wall thickness (see Figure 1). When the temperature of the wall increases, the
276 vertical strain increases by the thermal expansion. As the boundary condition at base of the domain
277 was vertically fixed, the deformation of the wall could only expand upward. On the left-hand side,
278 the heating rate is higher (so during the first 20 h), thermal expansion on the left-hand side is
279 higher than the right-hand side. This thermal expansion in the left-hand side was then "restrained"
280 by the right-hand side of the wall. At the same time, the vertical expansion of the wall mobilizes
281 the shaft friction along its interface in contact with the soil mass. That mobilized shaft friction
282 tends to prevent the wall vertical expansion, increasing then the vertical stress inside the wall. On
283 the other hand, the sensors located at larger depths (1.67 m) are subjected to higher increase of
284 vertical stress. That explains the compression of the wall during the first hours on the left-hand
285 side at large depths and tensile stress on the right-hand side.

286

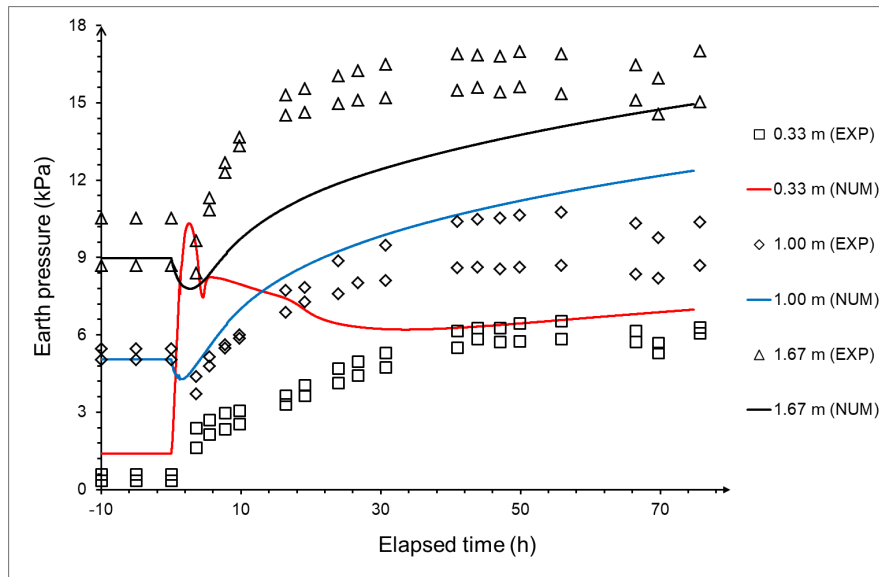
287 Figure 7 shows the normal stress on soil-wall interface versus elapsed time at various locations.
288 The initial value of the lateral earth pressure is approximately 1 kPa at 0.33 m depth, 5 kPa at 1.00
289 m depth and 9 kPa at 1.67 m depth. On the left-hand side (Figure 7a), at 0.33-m depth, there is
290 only one transducer. The measurement shows a quick increase of the earth pressure following the
291 heating phase, and the value at stabilization is approximately 4 kPa. At 1.00-m depth, there are
292 two sensors both showing a quick increase of the earth pressure and the final values are
293 approximately 11 kPa. The discrepancies between the two sensors are around 1 kPa. The sensors

294 at 1.67-m depth show similar trend with the final values close to 16 kPa. As a conclusion, for the
 295 left-hand side, the variation of earth pressure is more significant at greater depth during heating.



296
 297

(a)



298
 299

(b)

300 Fig.7 Stress versus elapsed time at various depths on the left-hand side (a) and on the right-
 301 hand side (b).

302

303 The general trend observed on the right-hand side is different at the start of heating (Figure 7b).
304 At 0.33-m depth, the two earth pressure sensors show quick increase with the heating and the final
305 average value equals 6 kPa, with a discrepancy of less than 0.5 kPa. At 1.00-m depth, both sensors
306 show first a decrease of the earth pressure during the first hours of heating. These values increase
307 and reach around 9 kPa at the end (with a discrepancy of 1 kPa). For the sensors at 1.67-m depth,
308 the earth pressure increases with the heating and reaches 15 -17 kPa at the end. It could be seen
309 there are still increase of pressure on both side at end of the test, this may due to a minor problem
310 with the measurement.

311

312 The numerical results corresponding to the sensors at 1.00-m and 1.67-m depths show good
313 agreement with the experimental ones for both sides. Even the decrease of the earth pressure at
314 1.00-m depth on the right-hand side was well predicted. However, the numerical results
315 corresponding to lower depth (0.33 m) are significantly different from the experiment values. On
316 the left-hand side, the numerical simulation shows a decrease of earth pressure during the first
317 hour, which was not observed in the experiment. On the right-hand side, the earth pressure spikes
318 during the first hour, which was not observed in the experiment. These problems would be
319 explained by the mechanical behavior of the sand in higher deflections [36, 39] under low stress
320 level that could not be well predicted by FEA. This could also explain why was there reasonable
321 accord before heating.

322

323 In order to better understand the results on the change of earth pressure (shown in Figure 7), the
 324 deformed mesh (5 h after the starting of the heating) is shown in Figure 8. Heating induces thermal
 325 expansion of the wall. That tends to increase the earth pressure at the soil/wall interface. However,
 326 as the pipes were located closer to the left-hand side, the temperature distribution is non-uniform.
 327 With the temperature on the left-hand side increasing more quickly than that on the right-hand
 328 side. This induces a bending of the wall that can be seen clearly in the Figure 9. This bending
 329 contributes also to the modification of the earth pressure. Besides the increase of earth pressure
 330 related to the wall expansion, the wall bending decreases the earth pressure (mostly on the top) on
 331 the left-hand side and increases that on the right-hand side. That explains why the increase of earth
 332 pressure at 0.33-m depth on the right-hand side is higher than those at higher depth and the order
 333 is opposite on the left-hand side. In addition, the bending of the wall also explains the decrease of
 334 earth pressure observed at 1.00-m depth on the right-hand side during the first few hours.

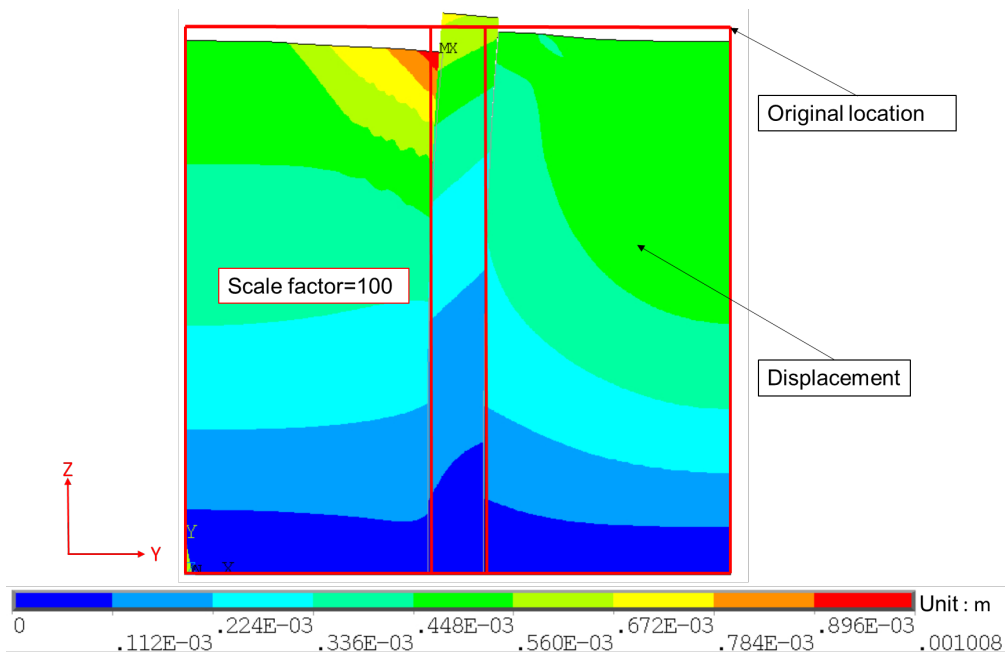


Fig.8 Deformed mesh at 5 hours (the color represents the sum of Y and Z displacement

337 vectors).

338

339 **5. Discussion**

340 In the present work, a 1-g physical model was used to study the thermo-mechanical behavior of
341 an energy wall panel. Strainmeters were used to capture the axial strain inside the wall and earth
342 pressure transducers were used to capture the normal stress at the soil/wall interface. This
343 approach has been used in various studies to investigate the mechanical behavior of geostructures
344 [40-42]. The results obtained in the present work show that this method could be also used to
345 investigate the thermo-mechanical behavior of energy geostructures.

346

347 As far as the numerical model was concerned, the present study used a plane strain 2D FE model
348 that approximates the conditions of the experiment. Even if this model could not capture the 3D
349 heterogeneity of the temperature distribution, related to the difference between the inlet and outlet
350 temperatures, a generally good agreement between the numerical and the experimental results can
351 be observed. This confirms also that the boundary conditions and the constitutive laws used in
352 this model are suitable for this case. Note that, for studying the thermal behavior of energy
353 geostructures, usually only heat conduction is considered for heat transfer in the soil and in the
354 reinforce concrete [29, 30, 43] unless ground water flow is present [7, 44, 45]. Heat convection in
355 heat exchange pipe was discussed in the literature [32] and the heat transfer mechanism between
356 the fluid and the pipe is more complex to be simulated [46, 47]. The hypothesis of elastic
357 deformation is usually used for gravel soils in numerical simulation because it is in agreement

358 with experimental observations [27, 29, 48, 49]. In some cases where clayey soils were considered,
359 more complex constitutive laws maybe required [50-53]. As mentioned above, to simplify the
360 model, the heat exchange pipe is often represented by a line with controlled temperature [26]; The
361 thermo-mechanical behavior of the soil was assumed to be elastic and the effect of temperature
362 on the soil mechanical properties was ignored.

363

364 Both numerical and experimental results obtained in the present work evidence that heating the
365 diaphragm wall induces thermal expansion and this increases the lateral earth pressure applied on
366 the wall surface. The lateral earth pressure could be three times larger than the initial stress value
367 under low stress level. This variation seems to have a significant contribution to the vertical stress
368 within the wall. Previous studies on energy pile indicate that radial contact pressures typically
369 increase less than 5 kPa along 20 m depth of the pile under an increase of 25°C of the pile
370 temperature [33, 34]. In real scale structures, the height to width ratio could be much higher than
371 the ratio in this physical study (equal to 10). As a result, the increase of lateral earth pressures
372 might be negligible with respect to the variations of vertical stresses. However, for an energy pile,
373 the increase of this pressure is almost homogenous because the layout of the pipes is usually
374 symmetric. For diaphragm walls, the behavior is more complex and strongly depends on the
375 distribution of the heat exchange pipes inside the wall. The eccentric position of the heat
376 exchanger loop caused a temperature gradient across the wall thickness, which leads to wall
377 bending. This phenomenon exists also in the wall that is not fully embedded [31], since the
378 temperature condition on the soil side is different from the temperature condition on the

379 excavation side. This represents an additional contribution to thermally-induced vertical strains
380 that are not uniform on the two sides of the wall.

381

382 **6. Conclusions**

383 The thermo-mechanical behavior of energy wall panel during heating was investigated using both
384 physical and numerical models. The following conclusions can be drawn:

385

- 386 - Heating induces thermal expansion of the wall. The vertical thermal expansion mobilizes the
387 shaft friction between the soil and the wall and then modifies the axial stress state inside the
388 wall. Horizontal expansion increases the earth pressure at the soil/wall interface, and thus
389 increases the mobilized shaft friction along the wall and the vertical stress inside the wall.
- 390 - As the pipe layout was not symmetric, thermal expansion bends the wall resulting in different
391 stress/strain response between the two sides.
- 392 - A short-term heating of the wall shows a significant temperature gradient across the wall
393 thickness. As a result, significant stress/strain variation is generated within the wall during
394 the first few hours.
- 395 - The numerical model using an elastic law for the thermo-mechanical behavior of soil is
396 appropriate to predict the behavior of the wall under thermal loading. There is however some
397 discrepancy between experiment and numerical results that requires a deeper investigation,
398 i.e. soil behavior at low stress level, 3D effect in the numerical model, etc.

399 - In spite of the temperature difference between the outlet and inlet fluid temperature, that
400 induced a non-uniform temperature distribution inside the wall, a 2D numerical model seems
401 appropriate to predict the main features of the panel's thermo-mechanical behavior observed
402 by physical model.

403

404 **Acknowledgement**

405 This research was supported by the National Natural Science Foundation of China (grant
406 number 41272314); and Science and Technology Project of Suzhou (grant number
407 SYG201451); and the European Commission via the Marie Curie IRSES project GREAT
408 'Geotechnical and geological Responses to climate change: Exchanging Approaches and
409 Technologies on a world-wide scale' (grant number FP7-PEOPLE-2013-IRSES-612665).
410 Thanks are also due to Yinkang Zhou from Nanjing University for valuable discussion.

411

412 **Reference**

- 413 [1] Brandl H (2006) Energy foundations and other thermo-active ground structures.
414 GEOTECHNIQUE 56(2): 81-122. doi: 10.1680/geot.2006.56.2.81
- 415 [2] Laloui L, Nuth M (2008) Investigations on the mechanical behaviour of a Heat Exchanger
416 Pile. In: Deep Foundations On Bored And Auger Piles, Proceedings (No. LMS-CONF-2009-
417 003, pp 343-347). Crc Press-Taylor & Francis Group, 6000 Broken Sound Parkway Nw, Ste
418 300, Boca Raton, Fl 33487-2742 Usa.
- 419 [3] Chuang YU, Pan LY, Liu SY, Cai YQ (2009) Working mechanism and application of heat

- 420 exchanger piles. *Yantu Lixue/rock & Soil Mechanics* 30(4):932-937. (In Chinese)
- 421 [4] Péron H, Knellwolf C, Laloui L (2011) A method for the geotechnical design of heat
422 exchanger piles In: *Proceedings of the Geo-Frontiers 2011 Conference*, Jie H, Daniel E,
423 Alzamora, PE ASTM, *Geotechnical Special Publications (GSP)* 211:470-479.
- 424 [5] Boënnec O (2009) Piling on the Energy. *Geodrilling International* 150:25-8.
- 425 [6] Dupray F, Li C, Laloui L (2014) Heat-exchanger piles for the de-icing of bridges. *Acta*
426 *Geotech* 9:413-423. doi: 10.1007/s11440-014-0307-2
- 427 [7] Suryatriyastuti ME, Mroueh H, Burlon S (2013) Impact of transient heat diffusion of a
428 thermoactive pile on the surrounding soil. In: Laloui L, Di Donna A (eds.) *Energy*
429 *Geostructures: Innovation in Underground Engineering*. ISTE Ltd. and John Wiley & Sons
430 Inc, 193-209.
- 431 [8] Kürten S, Mottaghy D, Ziegler M (2015) A new model for the description of the heat transfer
432 for plane thermo-active geotechnical systems based on thermal resistances. *Acta Geotech*
433 10:219-229. doi: 10.1007/s11440-014-0311-6
- 434 [9] Laloui L, Nuth M, Vulliet L (2006) Experimental and numerical investigations of the
435 behaviour of a heat exchanger pile. *Int J Numer Anal Met* 30(8):763-781. doi:
436 10.1016/S1571-9960(05)80040-0
- 437 [10] Bourne-Webb PJ, Amatya B, Soga K, et al (2009) Energy pile test at Lambeth College,
438 London: geotechnical and thermodynamic aspects of pile response to heat cycles.
439 *Géotechnique* 59(3):237. doi: 10.1680/geot.2009.59.3.237
- 440 [11] McCartney JS, Murphy KD (2012) Strain Distributions in Full-Scale Energy Foundations

- 441 (DFI Young Professor Paper Competition 2012). DFI Journal-The Journal of the Deep
442 Foundations Institute 6(2):26-38. doi:10.1179/dfi.2012.008
- 443 [12] Murphy KD, McCartney JS, Henry KS (2015) Evaluation of thermo-mechanical and
444 thermal behavior of full-scale energy foundations. *Acta Geotech* 10(2):179-195. doi:
445 10.1007/s11440-013-0298-4
- 446 [13] Laloui L, Cekerevac C (2008) Non-isothermal plasticity model for cyclic behaviour of soils.
447 *Int J Numer Anal Met* 32(5): 437-460. doi:10.1002/nag.629
- 448 [14] McCartney JS, Rosenberg JE, Sultanova A (2010) Engineering performance of thermo-
449 active foundation systems. In: Goss CM, Kerrigan JB, Malamo J, McCarron MO, Wiltshire
450 RL (eds) *GeoTrends: the Progress of Geological and Geotechnical Engineering in Colorado*
451 *at the Cusp of a New Decade (GPP 6)*, 27–42.
- 452 [15] McCartney JS, Rosenberg JE (2011) Impact of heat exchange on the axial capacity of
453 thermo-active foundations. In: Han J, Alzamora DE (eds) *Proceedings of geo-frontiers 2011*
454 (GSP 211). ASCE, Reston, VA, 488–498
- 455 [16] Kalantidou A, Tang AM, Pereira J-M, Hassen G (2012) Preliminary study on the
456 mechanical behaviour of heat exchanger pile in physical model. *Géotechnique*
457 62(11):1047-1051. doi: 10.1680/geot.11.T.013
- 458 [17] Stewart MA, McCartney JS (2013) Centrifuge modeling of soil-structure interaction in
459 energy foundations. *J Geotech Geoenviron* 140(4):04013044. doi:
460 10.1061/(ASCE)GT.1943-5606.0001061
- 461 [18] Yavari N, Tang AM, Pereira J-M, Hassen G (2014) Experimental study on the mechanical

- 462 behaviour of a heat exchanger pile using physical modelling. *Acta Geotech* 9(3):385-398.
463 doi: 10.1007/s11440-014-0310-7
- 464 [19] Kramer CA, Ghasemi-Fare O, Basu P (2015) Laboratory thermal performance tests on a
465 model heat exchanger pile in sand. *Geotech Geol Eng* 33(2):253-271. doi: 10.1007/s10706-
466 014-9786-z
- 467 [20] Goode III JC, McCartney JS (2015) Centrifuge modeling of end-restraint effects in energy
468 foundations. *J Geotech Geoenviron* 141(8):04015034. doi: 10.1061/(ASCE)GT.1943-
469 5606.0001333
- 470 [21] Yavari N, Tang A.M, Pereira, J-M, Hassen G (2016) Mechanical behaviour of a small-scale
471 energy pile in saturated clay. *Géotechnique* 66(11):878-887. doi:10.1680/geot./15-T-026
- 472 [22] Yavari N, Tang AM, Pereira J-M, Hassen G (2016) Effect of temperature on the shear
473 strength of soils and soil/structure interface. *Can Geotech J* 53(7):1186-1194. doi:
474 10.1139/cgj-2015-0355
- 475 [23] Nguyen VT, Tang AM, Pereira J-M (2017) Long-term thermo-mechanical behavior of
476 energy pile in dry sand. *Acta Geotech* 1-9. doi:10.1007/s11440-017-0539-z
- 477 [24] Laloui L, Nuth M (2005) Numerical modelling of the behaviour of a heat exchanger pile.
478 *Revue européenne de génie civil* 9(5-6): 827-839.
- 479 [25] Rotta Loria AF, Gunawan A, Shi C, et al (2015) Numerical modelling of energy piles in
480 saturated sand subjected to thermo-mechanical loads. *Geomech Eng En* 1:1-15.
481 doi:10.1016/j.gete.2015.03.002
- 482 [26] Yavari N, Tang AM, Pereira JM, et al (2014) A simple method for numerical modelling of

- 483 energy pile's mechanical behavior. *Géotechnique Lett* 4(April-June):119-124. doi:
484 10.1680/geolett.13.00053
- 485 [27] Suryatriyastuti ME, Mroueh H, Burlon S (2012) Understanding the temperature-induced
486 mechanical behaviour of energy pile foundations. *Renew Sust Energ Rev* 16(5): 3344-3354.
487 doi:10.1016/j.rser.2012.02.062
- 488 [28] Salciarini D, Ronchi F, Cattoni E, et al (2013) Thermomechanical effects induced by energy
489 piles operation in a small piled raft. *Int J Geomech* 15(2):04014042.
490 doi:10.1061/(ASCE)GM.1943-5622.0000375.
- 491 [29] Gashti EHN, Malaska M, Kujala K (2014) Evaluation of thermo-mechanical behaviour of
492 composite energy piles during heating/cooling operations. *Eng Struct* 75:363-373.
493 doi:10.1016/j.engstruct.2014.06.018
- 494 [30] Amatya BL, Soga K, Bourne-Webb PJ, et al (2012) Thermo-mechanical behaviour of
495 energy piles. *Géotechnique* 62(6): 503-519. doi:10.1680/geot.10.P.116
- 496 [31] Bourne-Webb PJ, Freitas TMB, da Costa Gonçalves RA (2016) Thermal and mechanical
497 aspects of the response of embedded retaining walls used as shallow geothermal heat
498 exchangers. *Energ Buildings* 125:130-141. doi: 10.1016/j.enbuild.2016.04.075
- 499 [32] Sterpi D, Coletto A, Mauri L (2017) Investigation on the behaviour of a thermo-active
500 diaphragm wall by thermo-mechanical analyses. *Geomech Eng En* 9:1-20. doi:
501 10.1016/j.gete.2016.10.001
- 502 [33] Olgun CG, Ozudogru TY, Arson CF (2014) Thermo-mechanical radial expansion of heat
503 exchanger piles and possible effects on contact pressures at pile–soil interface.

504 Géotechnique Lett 4(3):170-178. doi:10.1680/geolett.14.00018

505 [34] Ozudogru TY, Olgun CG, Arson CF (2015) Analysis of friction induced thermo-mechanical
506 stresses on a heat exchanger pile in isothermal soil. Geotech Geol Eng 33(2):357-371.
507 doi:10.1007/s10706-014-9821-0

508 [35] Yin S, Towler BF, Dusseault MB, et al (2009) Numerical experiments on oil sands shear
509 dilation and permeability enhancement in a multiphase thermoporoelastoplasticity
510 framework. J Petrol Sci Eng 69(3):219-226. doi:10.1016/j.petrol.2009.08.017

511 [36] Karthigeyan S, Ramakrishna V, Rajagopal K (2006) Influence of vertical load on the lateral
512 response of piles in sand. Comput Geotech 33(2):121-131.
513 doi:10.1016/j.compgeo.2005.12.002

514 [37] Allan ML (2000) Materials characterization of superplasticized cement–sand grout.
515 Cement Concrete Res 30(6):937-942. doi:10.1016/S0008-8846(00)00275-1

516 [38] Hazzar L, Nhussien M, Karray M (2017) Influence of vertical loads on lateral response of
517 pile foundations in sands and clays. Journal of Rock Mechanics and Geotechnical
518 Engineering 9(2):291-304. doi: 10.1016/j.jrmge.2016.09.002

519 [39] Hussien MN, Tobita T, Iai S, et al (2014) On the influence of vertical loads on the lateral
520 response of pile foundation. Comput Geotech 55(1):392-403. doi:
521 10.1016/j.compgeo.2013.09.022

522 [40] Reddy SB, Krishna AM (2015) Recycled Tire Chips Mixed with Sand as Lightweight
523 Backfill Material in Retaining Wall Applications: An Experimental Investigation. Int J of
524 Geosynth and Ground Eng 1(4):31. doi:10.1007/s40891-015-0036-0

- 525 [41] Lee KH, Cho JY, Salgado R, Lee I (2001) Retaining wall model test with waste foundry
526 sand mixture backfill, *Geotech Test J* 24:401–408. doi: 10.1520/GTJ11137J
- 527 [42] Schad H, Vermeer PA, Lächler A (2007) Fresh concrete pressure in diaphragm wall panels
528 and resulting deformations. In: Grosse, Ch. U. (Ed.): *Advances in Construction Materials*,
529 Berlin: Springer Verlag, 2007:505-512.
- 530 [43] Sun M, Xia C, Zhang G (2013) Heat transfer model and design method for geothermal heat
531 exchange tubes in diaphragm walls. *Energ Buildings* 61(6):250-259. doi:
532 10.1016/j.enbuild.2013.02.017
- 533 [44] Di Donna A, Barla M (2016) The role of ground conditions on energy tunnels' heat
534 exchange. *ICE Env. Geotech.*, 3, 214-224. doi:10.1680/jenge.15.00030
- 535 [45] Dupray F, Baehler M, Laloui L (2013) Effect of groundwater flow on the THM behavior
536 of an energy pile. *Proc. Int. Symp. Coupled Phenomena in Environmental Geotechnics*,
537 Turin (Italy), 483-489. doi:10.1201/b15004-63
- 538 [46] Dubroca B, Duffa G, Leroy B (2002, September) High Temperature Mass and Heat
539 Transfer Fluid-Solid Coupling. In *AIAA/AAAF 11th International Space Planes and
540 Hypersonic Systems and Technologies Conference*, 5124.
- 541 [47] Khoury RRE, Errera M, Khoury KE, et al (2017) Efficiency of coupling schemes for the
542 treatment of steady state fluid-structure thermal interactions. *Int J Therm Sci* 115:225–235.
543 doi: 10.1016/j.ijthermalsci.2017.02.001
- 544 [48] Jeong S, Lim H, Lee J K, et al (2014) Thermally induced mechanical response of energy
545 piles in axially loaded pile groups. *Appl Therm Eng* 71(1):608-615.

- 546 doi:10.1016/j.applthermaleng.2014.07.007
- 547 [49] Laloui L (2001) Thermo-mechanical behaviour of soils. *Revue Française De Génie Civil*
- 548 5(6):809–843.
- 549 [50] Cekerevac C, Laloui L (2004) Experimental study of thermal effects on the mechanical
- 550 behaviour of a clay. *Int J Numer Anal Met* 28(3):209-228. doi: 10.1002/nag.332
- 551 [51] Laloui L, Cekerevac C, François B (2005) Constitutive modelling of the thermo-plastic
- 552 behaviour of soils. *Revue Européenne De Génie Civil* 9(5-6):635-650.
- 553 [52] Tang AM, Cui YJ, Barnel N (2008) Thermo-mechanical behaviour of a compacted swelling
- 554 clay. *Géotechnique* 58(1):45-54. doi: 10.1680/geot.2008.58.1.45
- 555 [53] Hong PY, Pereira J-M, Tang AM, Cui YJ (2013) On some advanced thermo-mechanical
- 556 models for saturated clays. *Int J Numer Anal Met* 37:2952 – 2971. doi: 10.1002/nag.2170
- 557